

---

---

# Quantitative Imaging Biomarkers for $^{90}\text{Y}$ Distribution on Bremsstrahlung SPECT After Resin-Based Radioembolization

Isabel Schobert<sup>1,2</sup>, Julius Chapiro<sup>1</sup>, Nariman Nezami<sup>1</sup>, Charlie A. Hamm<sup>1,2</sup>, Bernhard Gebauer<sup>2</sup>, MingDe Lin<sup>1,3</sup>, Jeffrey Pollak<sup>1</sup>, Lawrence Saperstein<sup>1</sup>, Todd Schlachter<sup>1</sup>, and Lynn J. Savic<sup>1,2</sup>

<sup>1</sup>Department of Radiology and Biomedical Imaging, Yale School of Medicine, New Haven, Connecticut; <sup>2</sup>Institute of Radiology, Charité Universitätsmedizin Berlin, Corporate Member of Freie Universität Berlin, Humboldt-Universität, and Berlin Institute of Health, Berlin, Germany; and <sup>3</sup>Visage Imaging Inc., San Diego, California

---

Our purpose was to identify baseline imaging features in patients with liver cancer that correlate with  $^{90}\text{Y}$  distribution on postprocedural SPECT and predict tumor response to transarterial radioembolization (TARE). **Methods:** This retrospective study was approved by the institutional review board and included 38 patients with hepatocellular carcinoma (HCC) ( $n = 23$ ; 18/23 men; mean age,  $62.39 \pm 8.62$  y; 34 dominant tumors) and non-HCC hepatic malignancies ( $n = 15$ ; 9/15 men; mean age,  $61.13 \pm 11.51$  y; 24 dominant tumors) who underwent 40 resin-based TARE treatments (August 2012 to January 2018). Multiphasic contrast-enhanced MRI or CT was obtained before and Bremsstrahlung SPECT within 2 h after TARE. Total tumor volume ( $\text{cm}^3$ ) and enhancing tumor volume (ETV [ $\text{cm}^3$ ] and % of total tumor volume), and total and enhancing tumor burden (%), were volumetrically assessed on baseline imaging. Up to 2 dominant tumors per treated lobe were analyzed. After multimodal image registration of baseline imaging and SPECT/CT,  $^{90}\text{Y}$  distribution was quantified on SPECT as tumor-to-normal-liver ratio (TNR). Response was assessed according to RECIST1.1 and quantitative European Association for the Study of the Liver criteria. Clinical parameters were also assessed. Statistical tests included Mann-Whitney  $U$ , Pearson correlation, and linear regression. **Results:** In HCC patients, high baseline ETV% significantly correlated with high TNR on SPECT, demonstrating greater  $^{90}\text{Y}$  uptake in the tumor relative to the liver parenchyma ( $P < 0.001$ ). In non-HCC patients, a correlation between ETV% and TNR was observed as well ( $P = 0.039$ ). Follow-up imaging for response assessments within 1–4 mo after TARE was available for 23 patients with 25 treatments. The change of ETV% significantly correlated with TNR in HCC ( $P = 0.039$ ) but not in non-HCC patients ( $P = 0.886$ ). Additionally, Child–Pugh class B patients demonstrated significantly more  $^{90}\text{Y}$  deposition in nontumorous liver than Child–Pugh A patients ( $P = 0.021$ ). **Conclusion:** This study identified ETV% as a quantifiable imaging biomarker on preprocedural MRI and CT to predict  $^{90}\text{Y}$  distribution on postprocedural SPECT in HCC and non-HCC. However, the relationship between the preferential uptake of  $^{90}\text{Y}$  to the tumor and tumor response after radioembolization could be validated only for HCC.

**Key Words:** radioembolization;  $^{90}\text{Y}$ ; quantitative SPECT; contrast enhancement; imaging biomarker

**J Nucl Med 2019; 60:1066–1072**

DOI: 10.2967/jnumed.118.219691

---

**H**epatocellular carcinoma (HCC) is the sixth most common cancer and the third most common cause of cancer-related deaths worldwide (1). Moreover, liver is the primary metastatic site for many malignancies, especially of gastrointestinal origin such as colorectal carcinoma or neuroendocrine tumors (2). Over 70% of newly diagnosed patients with primary or secondary liver cancer present with advanced disease stages and are no longer amenable for curative therapeutic approaches (3,4). In this setting, intraarterial therapies such as transarterial chemoembolization (TACE) and radioembolization (TARE) with  $^{90}\text{Y}$  constitute mainstay palliative treatment options (5).

In TARE, microspheres loaded with radioactive  $^{90}\text{Y}$  are injected into the hepatic artery to deliver therapeutic doses of radiation to the liver lobe that contains the target tumors. The particles are trapped and remain in the tumor capillary bed, where they decay with  $\beta^-$ -emissions (6). Radiation is the predominant therapeutic effect of TARE, whereas the embolic properties of the 20- to 60- $\mu\text{m}$  microspheres remain limited and depend on the total number of administered microspheres. In fact, angiographic stasis before complete dose delivery occurs in only about 20% of treatments (7,8).

Previous studies have shown that  $^{90}\text{Y}$  uptake of the target tumors corresponds with tumor response to treatment (9). A clinically used tool to predict  $^{90}\text{Y}$  biodistribution before TARE is the preparatory  $^{99\text{m}}\text{Tc}$ -macroaggregated albumin ( $^{99\text{m}}\text{Tc}$ -MAA) scan. However, the prognostic value of  $^{99\text{m}}\text{Tc}$ -MAA for  $^{90}\text{Y}$  deposition patterns is limited mainly by different particle sizes and hemodynamics, which restricts the relevance of the  $^{99\text{m}}\text{Tc}$ -MAA scan to the identification of hepatopulmonary shunting (10).

For post-TARE evaluation of  $^{90}\text{Y}$  distribution in clinical practice, deposits are visualized on Bremsstrahlung SPECT immediately after treatment to qualitatively assess  $^{90}\text{Y}$  distribution to the tumor and liver tissue as well as nontarget deposition and shunting to other organs. More recently, quantitative methods for SPECT analysis have been investigated for the measurement of  $^{90}\text{Y}$  distribution and calculation of absorbed doses and proved technically feasible in an experimental setting (11). However, as  $^{90}\text{Y}$  uptake of tumors and dose–response relationships are highly variable across

---

Received Sep. 5, 2018; revision accepted Dec. 19, 2018.  
For correspondence or reprints contact: Julius Chapiro, Department of Radiology and Biomedical Imaging, Yale School of Medicine, 300 Cedar St., TAC N312A, New Haven, CT 06520.  
E-mail: julius.chapiro@yale.edu  
Published online Jan. 17, 2019.  
COPYRIGHT © 2019 by the Society of Nuclear Medicine and Molecular Imaging.

tumors of different etiology and morphology, the use of quantitative  $^{90}\text{Y}$ -SPECT for the prediction of tumor response to TARE remains challenging.

Therefore, this study aimed to identify and establish baseline imaging features in patients with liver malignancies that predict  $^{90}\text{Y}$  distribution as seen on post-TARE Bremsstrahlung SPECT and to assess the prognostic value of  $^{90}\text{Y}$  distribution for early prediction of tumor response.

## MATERIALS AND METHODS

### Study Cohort

This Health Insurance Portability and Accountability Act-compliant, retrospective single-center study was approved by the institutional review board, and informed consent was waived. In total, 38 patients with 23 HCC and 15 non-HCC liver malignancies who received lobar resin-based  $^{90}\text{Y}$ -TARE between August 2012 and January 2018 were included. The relatively high dropout rate due to missing SPECT was related to reimbursement system regulations that stipulated planar scans instead of SPECT. Forty treated liver lobes with 58 dominant tumors were included in the final analysis. With respect to partial-volume effect and limited spatial resolution of SPECT imaging, tumors smaller than 1.5 cm in diameter were excluded from the analysis (Fig. 1) (12). Clinical parameters were also assessed.

### MRI and CT Imaging

All patients received either MRI or CT of the liver before (baseline) and after 25 treatments 1–4 mo after the TARE procedure (follow-up). Scans were acquired according to the respective standardized institutional protocols. Specifically, patients underwent contrast-enhanced multiphase T1-weighted MRI with a 1.5-T scanner (Magnetom Avanto; Siemens) using a phased-array torso coil. The protocol included breath-hold unenhanced and contrast-enhanced (intravenous macrocyclic gadolinium) imaging in the hepatic arterial (20 s after administration), portal venous (70 s), and delayed phase (3 min). The

multiphase contrast-enhanced CT was performed with a multidetector scanner (Siemens) including native, arterial, portal venous, and delayed contrast-enhanced phases.

### TARE

Within 2 wk before TARE, all patients underwent mesenteric angiography to identify the vascular supply of the tumor and a  $^{99\text{m}}\text{Tc}$ -MAA scan to calculate the lung shunt fraction (LSF) and subsequent dose reduction.

For the actual treatment, a catheter was placed via transfemoral access under fluoroscopy guidance. Thereafter, a microcatheter was advanced into a proximal hepatic artery branch for lobar administration of  $^{90}\text{Y}$  resin-microspheres (SIR-Spheres; SIRTex Medical Limited). For bilobar therapy, the interval between sequential treatments was 3–4 wk.

### SPECT/CT

Within 2 h after completion of TARE, Bremsstrahlung SPECT/CT was performed. The dual-head scanner (Symbia TruePoint; Siemens) was equipped with a low-energy high-resolution collimator. Acquisition settings included 32 frames per camera and a 20-s acquisition time per frame. Matrix size was  $128 \times 128$ , and energy windows were 55–100 and 105–195 keV. The low-dose CT was acquired with 130 kV, 30 mAs, 0.8-s rotation time, and  $512 \times 512$  matrix. Maximum-likelihood reconstruction based on 3-dimensional (3D) ordered-subsets expectation maximization was performed using a manufacturer-specific software (FLASH 3D).

### 3D Tumor Assessment on MRI and CT

Up to 2 dominant target tumors per treated lobe were determined by size and segmented in 3 dimensions on the arterial-phase T1-weighted MRI or CT scans at baseline and follow-up using a semiautomated, volumetric technique to measure the total tumor volume (TTV,  $\text{cm}^3$ ). Quantitative European Association for the Study of the Liver (IntelliSpace Portal; Philips Healthcare), a software-based 3D quantification tool, was used to calculate the absolute enhancing tumor volume (ETV,  $\text{cm}^3$ ) and the ETV in percentage of the TTV (ETV%). Briefly, the precontrast scan was subtracted from the arterial-phase scan to remove background enhancement. The 3D segmented tumor mask was applied, and a reference region was placed in healthy liver parenchyma. Tumor enhancement was defined as 2 SDs above the signal intensity of the reference region as previously described (13). In addition, the treated liver lobes were segmented, and the total and enhancing tumor burden per treated lobe were assessed (14). These parameters are referred to here as imaging biomarkers for  $^{90}\text{Y}$  distribution.

For volumetric tumor response assessment, changes of TTV, ETV, and ETV% between baseline and follow-up imaging were calculated and interpreted according to the established qEASL% criteria (13,14). Additionally, tumor response was assessed according to RECIST1.1. Response was categorized as complete or partial response or as stable or progressive disease.

### $^{90}\text{Y}$ Biodistribution

$^{90}\text{Y}$  SPECT images were analyzed with a dedicated protocol in MIM Encore (MIM Software Inc.). Treated lobes and dominant tumors were volumetrically segmented on the baseline contrast-enhanced MRI or CT, which was nonrigidly registered to the CT of the SPECT/CT and then to the scatter- and attenuation-corrected SPECT. All remaining tumors in the treated lobe were also segmented, and the volumes were subtracted from the liver lobe volume to separate the healthy liver parenchyma from tumorous tissue. On the basis of these segmentations, the total number of counts in the dominant tumors and the nontumorous parenchyma of the treated lobe were quantified.  $^{90}\text{Y}$  activity per count was calculated on the basis of the administered dose, the LSF, and the total number of counts within the

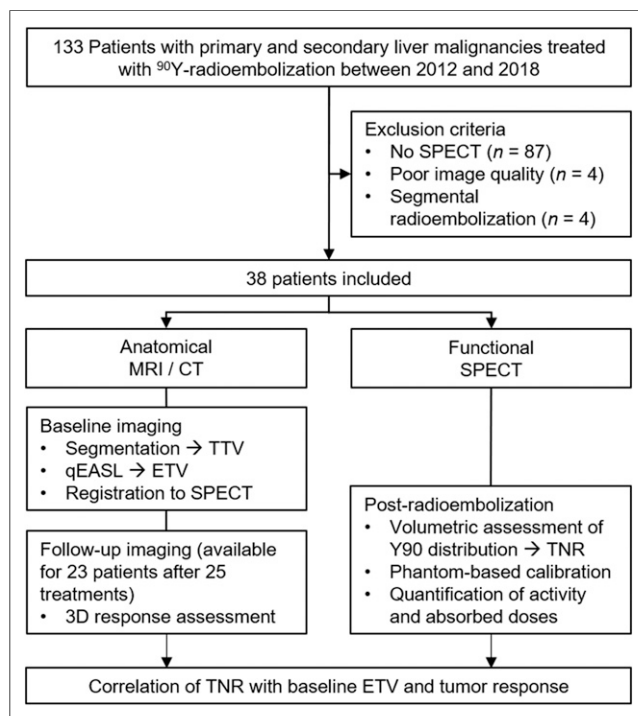


FIGURE 1. Study workflow and exclusion criteria.

**TABLE 1**  
Baseline HCC Patient Characteristics

Parameter	n (%)
<b>Demographics</b>	
Number of patients	23 (100)
Age (y), mean ± SD	62.39 ± 8.62
Male/female	18 (78.26)/5 (21.74)
<b>Ethnicity</b>	
Caucasian	18 (78.26)
Asian	1 (4.35)
African-American	4 (17.39)
<b>Disease characteristics</b>	
Etiology of cirrhosis	
Viral hepatitis	17 (73.91)
Alcohol consumption	4 (17.39)
Nonalcoholic steatohepatitis	2 (8.7)
Eastern Cooperative Oncology Group performance status	
0	11 (47.83)
1	12 (52.17)
Child–Pugh class	
A	13 (56.52)
B	10 (43.48)
Barcelona Clinic liver cancer stage	
B	10 (43.45)
C	13 (56.52)
Main portal vein thrombosis	5 (21.74)
Extrahepatic disease	3 (13.04)
Tumor characteristics, median (interquartile range, range)	
Number of tumors/liver	6 (3.5–12, 1–54)
Number of tumors/analyzed lobe	4 (2–5, 1–11)
TTV (cm <sup>3</sup> )/analyzed lobe	110.08 (79.82–225.58, 4.13–730.37)
ETV (cm <sup>3</sup> )/analyzed lobe	62.57 (7.47–112.8, 0–509.95)
Tumor burden (%)/analyzed lobe	13.05 (5.12–28.78, 0.71–67.56)
Enhancing tumor burden (%)/analyzed lobe	4.34 (0.83–12.41, 0–57.82)
Previous treatments	
Sorafenib	5 (21.74)
Resection*	3 (13.04)
TACE*	11 (47.83)
Ablation*	5 (21.74)
Other	5 (21.74)

\*Pretreated tumors are not included in the analysis.

**TABLE 2**  
Baseline Non-HCC Patient Characteristics

Parameter	n (%)
<b>Demographics</b>	
Number of patients	15 (100)
Age (y), mean ± SD	61.13 ± 11.51
Male/female	9 (60)/6 (40)
<b>Ethnicity</b>	
Caucasian	12 (80)
Asian	1 (6.67)
African-American	2 (13.33)
<b>Disease characteristics</b>	
Tumor entity	
Intrahepatic cholangiocarcinoma	2 (13.33)
Neuroendocrine cancer metastases	7 (46.67)
Colorectal cancer metastases	3 (20)
Melanoma cancer metastases	1 (6.67)
Prostate cancer metastases	1 (6.67)
Leiomyosarcoma metastases	1 (6.67)
Eastern Cooperative Oncology Group performance status	
0	9 (60)
1	6 (40)
Main portal vein thrombosis	1 (6.67)
Tumor characteristics, median (interquartile range, range)	
Number of tumors/liver	11 (5.5–11, 4–129)
Number of tumors/analyzed lobe	6 (3.5–6, 1–85)
TTV (cm <sup>3</sup> )/analyzed lobe	102.01 (67.03–300.89, 14.94–1,868.39)
ETV (cm <sup>3</sup> )/analyzed lobe	66.66 (19.54–87.79, 0–839.01)
Tumor burden/analyzed lobe (%)	6.1 (5.59–26.73, 1.53–76.86)
Enhancing tumor burden/analyzed lobe (%)	4.38 (2.12–5.45, 0–38.25)
Previous treatments	
Systemic therapies	10 (66.67)
Resection*	3 (20)
TACE*	1 (6.67)
Ablation*	2 (13.33)

\*Pretreated tumors are not included in the analysis.

liver. Finally, the tumor-to-normal-liver ratio (TNR) was calculated, representing the distribution of <sup>90</sup>Y between the dominant tumors and nontumorous liver in the treated lobe.

To convert the count-rate on the SPECT image to a measure of activity concentration, a phantom-based calibration correction factor was calculated of 4 phantom studies as previously described (11). Briefly, activity concentrations measured on SPECT were divided by

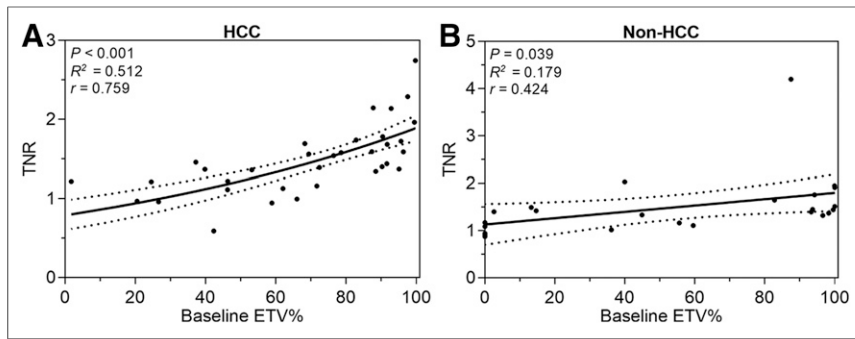


**FIGURE 2.** Correlation of baseline ETV% and  $^{90}\text{Y}$  distribution after TARE. This graph demonstrates that with greater ETV% on baseline imaging,  $^{90}\text{Y}$  uptake of tumor measured as TNR increases in HCC ( $n = 34$ ,  $P < 0.001$ ) (A) as well as non-HCC ( $n = 24$ ,  $P = 0.039$ ) (B). Intermittent lines indicate 95% confidence interval.

the true activity concentrations measured at the time of the scan using an activity meter to obtain the calibration correction factor (Supplemental Fig. 1; supplemental materials are available at <http://jnm.snmjournals.org>). The 4 results were averaged and multiplied by the counts within the volume of interest. Eventually, absorbed doses were calculated using partition modeling (15).

### Statistical Analysis

Descriptive results are reported as frequency ( $n$ , %), mean  $\pm$  SD, or median and range. Further analyses included Pearson correlation, linear regression, Mann–Whitney  $U$  test, and Kaplan–Meier curves. Statistical analyses were performed using SPSS (IBM Corp., version 24.0) and Prism (version 7.0). A  $P$  value of less than 0.05 was considered statistically significant.

## RESULTS

### Study Population and Survival Analysis

Detailed characteristics of the patient population are displayed in Tables 1 and 2. Patients with HCC and non-HCC had a median survival of 14.4 (1.58–55.76) and 18.97 (1.48–55.07) months after TARE, respectively. Five patients with HCC and 10 patients with non-HCC were still alive at the end of follow-up and censored for Kaplan–Meier analysis.

### Imaging Findings

**Baseline Imaging Features.** The tumor characteristics on baseline MRI or CT are displayed in Tables 1 and 2. The dominant

tumors measured  $5.24 \pm 2.93$  cm and  $4.68 \pm 2.48$  cm ( $P = 0.445$ ) for HCC and non-HCC, respectively.

**Response Assessment.** Follow-up imaging was acquired within a median time of 68 (30–111) and 78 (28–143) days for HCC and non-HCC, respectively, and was available after 25 treatments. According to 3D enhancement-based qEASL%, which was further used for correlation analyses with TNR, TARE achieved no complete responses, 0 and 2 (28.57%) partial responses, 17 (94.44%) and 5 (71.43%) stable disease, and 1 (5.56%) and 0 progressive disease in HCC and non-HCC, respectively. According to RECIST1.1, there was no complete response, 2 (11.11%) and 3 (42.86%) partial responses, 15 (83.33%) and 4 (57.14%) stable disease, and 1 (5.56%) and 0 progressive disease in HCC and non-HCC, respectively.

**$^{90}\text{Y}$  Distribution on SPECT/CT and Absorbed Dose Calculations.** Patients had a mean  $^{99\text{m}}\text{Tc-MAA}$  LSF of  $6.6\% \pm 4.7\%$ . The mean administered activity was  $1.17 \pm 0.61$  GBq, and the mean absorbed tumor and healthy liver dose were  $52.52 \pm 31.8$  and  $39.94 \pm 22.4$  Gy, respectively. The mean  $^{90}\text{Y}$  distribution to the dominant tumors quantified as TNR was  $1.47 \pm 0.42$  in HCC and  $1.52 \pm 0.65$  in non-HCC.

### Correlation Analyses

**Correlation of Baseline Imaging Features with  $^{90}\text{Y}$  Distribution and Survival.** The 2-tailed Pearson analysis revealed a significant correlation between baseline ETV% and  $^{90}\text{Y}$  distribution on SPECT quantified as TNR, showing that more relative enhancement was associated with higher TNR in patients with HCC ( $P < 0.001$ ). The correlation coefficient ( $r$ ) was 0.759 and  $R^2$  was 0.516 in a linear regression model. In patients with liver cancer other than HCC, the correlation of baseline ETV% with TNR was not as strong as in HCC but still statistically significant ( $P = 0.039$ ;  $r = 0.424$ ;  $R^2 = 0.179$ ) (Fig. 2). Specifically, a baseline ETV% cutoff of 80% was empirically identified to provide the most significant separation of TNR values in HCC ( $P < 0.001$ ) and non-HCC patients ( $P = 0.014$ ), demonstrating higher mean TNR for patients with ETV% of at least 80% (Fig. 3). As for the remaining baseline tumor characteristics, TTV ( $P = 0.109$  and 0.982), ETV ( $P = 0.43$  and 0.686), diameter ( $P = 0.488$  and 0.845), tumor burden ( $P = 0.498$  and 0.125), and enhancing tumor burden ( $P = 0.852$  and 0.768) did not demonstrate significant correlations with TNR. Of note, survival did not correlate with baseline ETV% in HCC ( $P = 0.088$ ) and non-HCC ( $P = 0.172$ ).

**Correlation of Baseline Clinical Features with  $^{90}\text{Y}$  Distribution.** To assess the effect of liver cirrhosis on the  $^{90}\text{Y}$  distribution, Child–Pugh classes were correlated with TNR. In the present cohort, the mean TNR of Child–Pugh B patients was significantly lower than that of Child–Pugh A patients ( $P = 0.021$ ) (Fig. 4). Furthermore, patients with Child–Pugh B had a significantly higher LSF than Child–Pugh A ( $P = 0.049$ ).

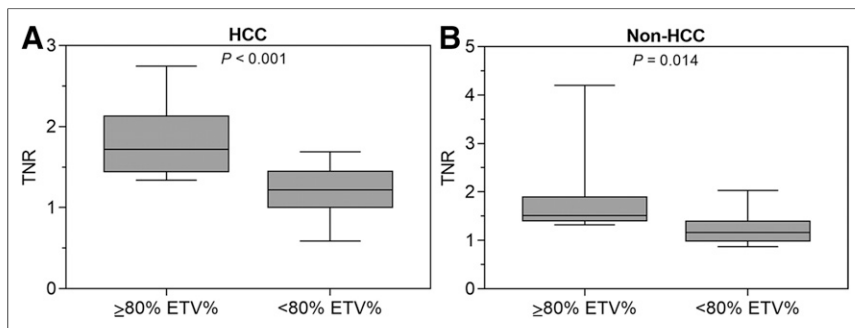


**FIGURE 3.** Stratification of  $^{90}\text{Y}$  distribution according to tumor enhancement thresholds. Mann–Whitney– $U$  test reveals 80% baseline ETV% as empirically most significant cutoff value to stratify patients with HCC ( $P < 0.001$ ) (A) and non-HCC ( $P = 0.014$ ) (B) according to TNR. Graph shows median, range, and 25th–75th percentiles.

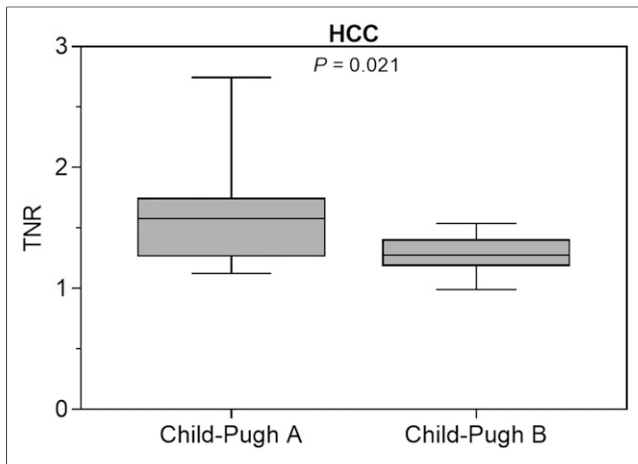


**FIGURE 4.** Stratification of  $^{90}\text{Y}$  distribution according to Child–Pugh class. HCC patients with Child–Pugh B show significantly decreased TNR compared with Child–Pugh A ( $P = 0.021$ ). Graph shows median, range, and 25th–75th percentiles.

*Correlation of  $^{90}\text{Y}$  Distribution with Tumor Response.* Furthermore,  $^{90}\text{Y}$  distribution was correlated with tumor response available in a subset of patients ( $n = 25$ ). For HCC, a high TNR correlated with tumor response according to the enhancement-based volumetric qEASL% criteria ( $P = 0.038$ ,  $R^2 = 0.216$ ,  $r = -0.465$ ) (Fig. 5). However, in non-HCC, no correlation was observed between TNR and tumor response according to qEASL% ( $P = 0.886$ ,  $R^2 = 0.002$ ,  $r = 0.044$ ) (Fig. 6).

There was no correlation between TNR and survival in HCC ( $P = 0.526$ ) or non-HCC patients ( $P = 0.233$ ).

## DISCUSSION

The main finding of this study is the identification of ETV% as a quantifiable imaging biomarker on preprocedural MRI and CT, which predicts  $^{90}\text{Y}$  distribution as measured on immediate post-procedural SPECT. Second, this study validated the relationship between the preferential uptake of  $^{90}\text{Y}$  activity to the tumor and tumor response after TARE in patients with HCC.

Recently, TARE was called into question when published results from prospective clinical trials comparing TARE with sorafenib as the standard of care in advanced HCC revealed no difference in

survival between both treatments (16,17). However, patient selection for TARE in those studies was based mainly on general clinical evaluations rather than individual tumor characteristics. This reflects the currently immature patient selection process in clinical practice, where TARE is oftentimes performed when patients are considered ineligible or not responding to other locoregional therapies such as TACE, which underscores the need for personalized and tumor-specific treatment indications. In this study, the ETV%, reflecting on pathologic tumor viability and vascularity, was identified as a noninvasive imaging biomarker and predictor for  $^{90}\text{Y}$  distribution to the tumor after TARE ( $P < 0.001$ ). Thus, the results of this study may help refine patient selection criteria for TARE, consolidating the role of TARE among other intraarterial therapies and improving treatment outcome with minimized toxicity by determining the patients who are most likely to benefit from TARE (18).

Previous studies have shown the feasibility and value of quantitative SPECT for the evaluation of the extra- and intrahepatic distribution of  $^{90}\text{Y}$  and absorbed dose quantifications after TARE (19). More recently, several studies investigating hepatic metastases found CT perfusion imaging and metabolic response assessment using PET predictive of tumor response early after TARE (20). This study introduces TNR as a quantitative surrogate on SPECT as a readily applicable predictor for enhancement-based tumor response after TARE in HCC ( $P = 0.038$ ). As morphologic changes of the tumors occur gradually and become measurable on anatomic imaging as late as 2–4 mo after TARE, TNR may thus allow for the evaluation of treatment efficacy immediately after treatment (21,22). Such immediate feedback can support timely clinical decision making in rapidly evolving disease processes of liver cancer in a palliative setting.

In addition to ETV% at baseline, the findings of this study suggest that liver cirrhosis represents an additional influencing factor on intrahepatic  $^{90}\text{Y}$  distribution. Liver cirrhosis not only is associated with worsened liver function but also causes fundamental structural changes to the parenchyma, with portal hypertension, arterioportal, and hepatovenous shunting being frequently encountered features (23). Such conditions may possibly explain why patients with Child–Pugh B demonstrated increased rates of non-target  $^{90}\text{Y}$  delivery ( $P = 0.021$ ) and higher LSF ( $P = 0.049$ ), while, in parallel, demonstrating decreased uptake in tumors, when compared with Child–Pugh A. The reduced dose delivered to the tumor necessarily results in lower response rates while simultaneously increasing the risk of radiation-induced injury to nontumorous parenchyma (24,25).

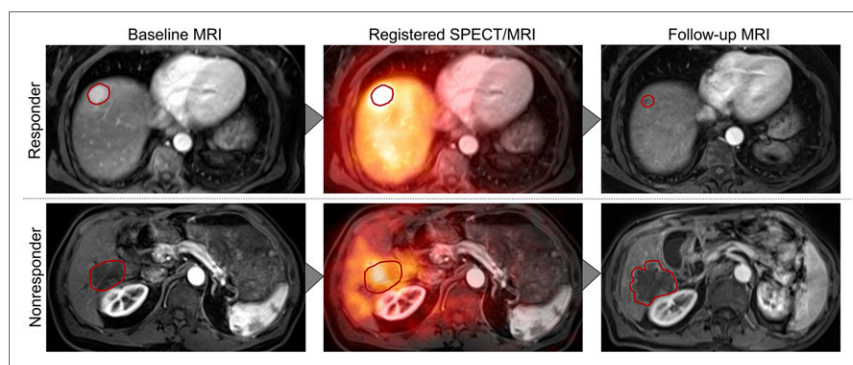


**FIGURE 5.** Multimodal image analysis. Postprocessing and analyses included volumetric segmentations of dominant tumors on baseline and follow-up MRI, registration of baseline MRI on postprocedural SPECT, and tumor response assessment.

The goal of high and tumor-specific dose delivery provided the rationale for the development of new therapeutic strategies with TARE (6). Among others, the concept of radiation segmentectomy was introduced, which represents a possibly curative approach applying high radiation doses to singular tumors restricted to a single or a few segments (26). Another approach, called boosted selective internal radiation therapy, targets patients with large HCC with or without portal vein thrombosis for personalized treatment intensification that entails increased amounts of administered  $^{90}\text{Y}$  activities (27). Patients were selected on the basis of their  $^{99\text{m}}\text{Tc}$ -MAA scan, quantifications of doses to the tumor and liver, and total injected dose. Boosted selective internal radiation

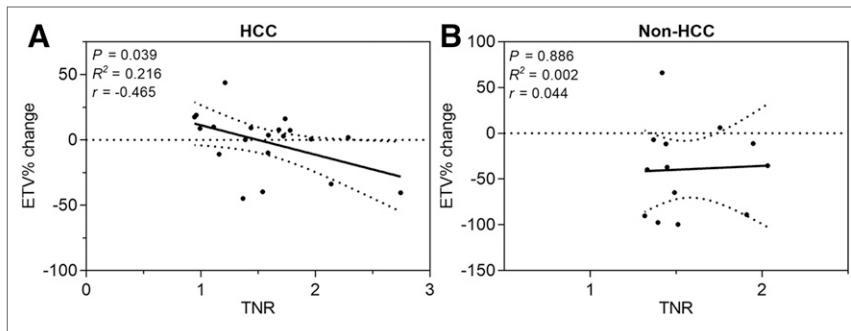


**FIGURE 6.** Correlation of  $^{90}\text{Y}$  distribution and changes of tumor enhancement after TARE. This graph demonstrates that  $^{90}\text{Y}$  uptake in dominant tumors correlates with reduction of ETV% according to qEASL tumor response criteria (available for 25 lobar treatments) in HCC ( $n = 20$ ) (A) but not in non-HCC ( $n = 13$ ) (B). Intermittent lines indicate 95% confidence interval.

therapy was found to achieve significantly higher tumor doses resulting in improved response rates without compromising patient safety. Although conducted with glass spheres containing higher activity per microsphere, this approach proves the potential and underscores the need for surrogate markers predicting  $^{90}\text{Y}$  distribution to achieve better outcomes after TARE.

Hepatic metastases usually show different contrast uptake and washout behavior than HCC (28,29). As the vascular density in metastatic tumors such as colorectal cancer metastases is usually lower than for HCC, metastases may lack contrast enhancement on baseline imaging and distinct alterations of contrast uptake dynamics throughout the course of TARE (22,28). In the present cohort, a high baseline ETV% was predictive of  $^{90}\text{Y}$  distribution to the tumor ( $P = 0.039$ ), but  $^{90}\text{Y}$  distribution did not correlate with tumor response ( $P = 0.886$ ). Thus, ETV% as an imaging biomarker for tumor-specific  $^{90}\text{Y}$  uptake and the dependent tumor response may be applied only for HCC.

This study had several limitations. This is a retrospective study with a relatively small sample size and relatively wide range of imaging intervals. Additionally, tumors of different entities were included in the non-HCC cohort, with potentially varying physiology and enhancement patterns that may affect the  $^{90}\text{Y}$  uptake behavior and response to TARE.

Finally, as compared with SPECT, PET may generally provide more advanced quantification techniques and superior spatial resolution (30). However, SPECT is currently still more widely available, with higher cost efficiency than PET, which provided the rationale to develop a quantitative SPECT approach in this study (31).

## CONCLUSION

This study showed the feasibility and prognostic value of ETV% as a quantifiable imaging biomarker on preprocedural MRI and CT, which predicts the relative  $^{90}\text{Y}$  distribution on postprocedural SPECT in HCC and non-HCC. However, the relationship between the preferential uptake of  $^{90}\text{Y}$  to the tumor and tumor response after TARE could be validated only for HCC. Overall, this study introduces an easily clinically applicable surrogate marker to refine and personalize patient selection for TARE.

## DISCLOSURE

Outside the submitted work, Lynn Savic reports grants from a Leopoldina Postdoctoral Fellowship and the Society of Interventional

Oncology (SIO); Julius Chapiro reports grants from the German–Israeli Foundation for Scientific Research and Development, Philips Healthcare, Boston Scientific, Guerbet, and SIO; MingDe Lin is a Visage Imaging employee; Lynn Savic, Julius Chapiro, and MingDe Lin report grants from the National Institutes of Health (NIH/NCI R01 CA206180); Isabel Schobert reports grants from the Biomedical Education Program (BMEP). No other potential conflict of interest relevant to this article was reported.

## ACKNOWLEDGMENTS

We thank Chi Liu, Brian Letzen, Sophie Antonia Stark, Paula Marie Oestmann, Clinton Wang, Adam Nelson, Neil Whiteside, Matt Gregory, Brian Patchell, Yanhong Deng, and Geliang Gan for their support and technical and statistical advice.

## REFERENCES

- Bray F, Ferlay J, Soerjomataram I, Siegel RL, Torre LA, Jemal A. Global cancer statistics 2018: GLOBOCAN estimates of incidence and mortality worldwide for 36 cancers in 185 countries. *CA Cancer J Clin*. 2018;68:394–424.
- Lozano R, Naghavi M, Foreman K, et al. Global and regional mortality from 235 causes of death for 20 age groups in 1990 and 2010: a systematic analysis for the global burden of disease study 2010. *Lancet*. 2012;380:2095–2128.
- Thomas MB, Zhu AX. Hepatocellular carcinoma: the need for progress. *J Clin Oncol*. 2005;23:2892–2899.
- Haddad AJ, Bani Hani M, Pawlik TM, Cunningham SC. Colorectal liver metastases. *Int J Surg Oncol*. 2011;2011:285840.
- Talenfeld AD, Sista AK, Madoff DC. Transarterial therapies for primary liver tumors. *Surg Oncol Clin N Am*. 2014;23:323–351.
- Kallini JR, Gabr A, Salem R, Lewandowski RJ. Transarterial radioembolization with yttrium-90 for the treatment of hepatocellular carcinoma. *Adv Ther*. 2016;33:699–714.
- Venkatarasimha N, Gogna A, Tong KTA, et al. Radioembolisation of hepatocellular carcinoma: a primer. *Clin Radiol*. 2017;72:1002–1013.
- Piana PM, Bar V, Doyle L, et al. Early arterial stasis during resin-based yttrium-90 radioembolization: incidence and preliminary outcomes. *HPB (Oxford)*. 2014;16:336–341.
- Badiyan S, Bhooshan N, Chuong MD, et al. Correlation of radiation dose and activity with clinical outcomes in metastatic colorectal cancer after selective internal radiation therapy using yttrium-90 resin microspheres. *Nucl Med Commun*. 2018;39:915–920.
- Liu DM, Salem R, Bui JT, et al. Angiographic considerations in patients undergoing liver-directed therapy. *J Vasc Interv Radiol*. 2005;16:911–935.
- Ito S, Kurosawa H, Kasahara H, et al.  $^{90}\text{Y}$  bremsstrahlung emission computed tomography using gamma cameras. *Ann Nucl Med*. 2009;23:257–267.
- Shady W, Sotirchos VS, Do RK, et al. Surrogate imaging biomarkers of response of colorectal liver metastases after salvage radioembolization using  $^{90}\text{Y}$ -loaded resin microspheres. *AJR*. 2016;207:661–670.
- Chapiro J, Wood LD, Lin M, et al. Radiologic-pathologic analysis of contrast-enhanced and diffusion-weighted MR imaging in patients with HCC after TACE: diagnostic accuracy of 3D quantitative image analysis. *Radiology*. 2014;273:746–758.
- Chapiro J, Duran R, Lin M, et al. Transarterial chemoembolization in soft-tissue sarcoma metastases to the liver: the use of imaging biomarkers as predictors of patient survival. *Eur J Radiol*. 2015;84:424–430.
- Mikell JK, Mahvash A, Siman W, Baladandayuthapani V, Mourtada F, Kappadath SC. Selective internal radiation therapy with yttrium-90 glass microspheres: biases and uncertainties in absorbed dose calculations between clinical dosimetry models. *Int J Radiat Oncol Biol Phys*. 2016;96:888–896.
- Vilgrain V, Abdel-Rehim M, Sibert A, et al; SARAH Trial Group. Radioembolisation with yttrium-90 microspheres versus sorafenib for treatment of advanced

- hepatocellular carcinoma (SARAH): study protocol for a randomised controlled trial. *Trials*. 2014;15:474.
17. Chow PHW, Gandhi M. Phase III multi-centre open-label randomized controlled trial of selective internal radiation therapy (SIRT) versus sorafenib in locally advanced hepatocellular carcinoma: the SIRveNIB study [abstract]. *J Clin Oncol*. 2017;35(suppl):4002.
  18. Piana PM, Gonsalves CF, Sato T, et al. Toxicities after radioembolization with yttrium-90 SIR-spheres: incidence and contributing risk factors at a single center. *J Vasc Interv Radiol*. 2011;22:1373–1379.
  19. Piasecki P, Narloch J, Brzozowski K, et al. The predictive value of SPECT/CT imaging in colorectal liver metastases response after <sup>90</sup>Y-radioembolization. *PLoS One*. 2018;13:e0200488.
  20. Shady W, Kishore S, Gavane S, et al. Metabolic tumor volume and total lesion glycolysis on FDG-PET/CT can predict overall survival after <sup>90</sup>Y radioembolization of colorectal liver metastases: a comparison with SUVmax, SUVpeak, and RECIST 1.0. *Eur J Radiol*. 2016;85:1224–1231.
  21. Riaz A, Kulik L, Lewandowski RJ, et al. Radiologic–pathologic correlation of hepatocellular carcinoma treated with internal radiation using yttrium-90 microspheres. *Hepatology*. 2009;49:1185–1193.
  22. Joo I, Kim H-C, Kim GM, Paeng JC. Imaging evaluation following <sup>90</sup>Y radioembolization of liver tumors: what radiologists should know. *Korean J Radiol*. 2018;19:209–222.
  23. Yu JS, Kim KW, Jeong MG, Lee JT, Yoo HS. Nontumorous hepatic arterial-portal venous shunts: MR imaging findings. *Radiology*. 2000;217:750–756.
  24. Kao Y-H, Steinberg JD, Tay Y-S, et al. Post-radioembolization yttrium-90 PET/CT: part 2—dose-response and tumor predictive dosimetry for resin microspheres. *EJNMMI Res*. 2013;3:57.
  25. Gabrielson A, Miller A, Banovac F, Kim A, He AR, Unger K. Outcomes and predictors of toxicity after selective internal radiation therapy using yttrium-90 resin microspheres for unresectable hepatocellular carcinoma. *Front Oncol*. 2015;5:292.
  26. Riaz A, Gates VL, Atassi B, et al. Radiation segmentectomy: a novel approach to increase safety and efficacy of radioembolization. *Int J Radiat Oncol Biol Phys*. 2011;79:163–171.
  27. Garin E, Lenoir L, Edeline J, et al. Boosted selective internal radiation therapy with <sup>90</sup>Y-loaded glass microspheres (B-SIRT) for hepatocellular carcinoma patients: a new personalized promising concept. *Eur J Nucl Med Mol Imaging*. 2013;40:1057–1068.
  28. Sica GT, Ji H, Ros PR. CT and MR imaging of hepatic metastases. *AJR*. 2000;174:691–698.
  29. Shah S, Shukla A, Paunipagar B. Radiological features of hepatocellular carcinoma. *J Clin Exp Hepatol*. 2014;4(suppl):S63–S66.
  30. Rahmim A, Zaidi H. PET versus SPECT: strengths, limitations and challenges. *Nucl Med Commun*. 2008;29:193–207.
  31. Hicks RJ, Hofman MS. Is there still a role for SPECT–CT in oncology in the PET–CT era? *Nat Rev Clin Oncol*. 2012;9:712–720.